

Supercooled Droplet Icing and Self-Jumping on Micro/nanostructured Surfaces: Role of Vaporization Momentum

Xiao Yan¹⁼, Samuel C. Y. Au¹⁼, Sui Cheong Chan¹, Ying Lung Chan¹, Ngai Chun Leung¹, Wa
Yat Wu¹, Dixon T. Sin¹, Guanlei Zhao², Casper H. Y. Chung¹, Mei Mei¹, Yinchuang Yang¹,
Huihe Qiu¹, Shuhuai Yao^{1*}

*¹Department of Mechanical and Aerospace Engineering, Hong Kong University of Science and
Technology, Hong Kong, China*

*²State Key Laboratory of Automotive Safety and Energy, School of Vehicle and Mobility, Tsinghua
University, Beijing 100084, China.*

⁼Equal contribution

** Corresponding author email: meshyao@ust.hk (Shuhuai Yao)*

ABSTRACT

Phase change under reduced environmental pressures is key to understanding liquid discharge and propulsion processes for aerospace applications. A representative case is the sessile water droplets exposed to high vacuum, which experience complex phase change and transport phenomena that behave so differently than that under the atmosphere. Here, we demonstrate a previously unexplored aspect of the mechanism governing icing droplet self-launching from superhydrophobic surfaces when exposed to low pressures (~ 100 Pa). In contrast to the previously reported recalescence-induced local overpressure underneath the droplet that propels icing droplet self-jumping, we show that the progressive recalescence over the free surface plays a significant role in droplet icing and jumping. The joint contribution of the top-down vaporization momentum and bottom-up local overpressure momentum leads to vaporization-compression-detaching dynamics of the freezing droplets. We delineate the jumping velocity of the icing droplet by analyzing droplet vaporization mediated by freezing and substrate structuring, and reveal jumping direction coupled with the spatially probabilistic ice nucleation. Our study provides new insights into phase change of supercooled droplets at extreme conditions seen in aerospace and vacuum industries.

Keywords: supercooled droplet, low pressure, evaporation, icing, superhydrophobic

Water droplet freezing on solid surfaces poses safety and economic threats to transportation infrastructure, power generation/transmission systems, and telecommunication facilities.¹⁻⁴ A classic example in the aerospace industry is the in-flight icing of supercooled droplets that has caused >40% of general aviation accidents.^{5,6} More recently, the global energy transition to renewable energies has exacerbated the issue of ice accretion on wind turbine blades and photovoltaic panels, which causes significant power loss and serious safety hazards.⁷⁻¹⁰

Icing of a droplet on solid surfaces starts from ice nucleation¹² followed by crystallization propagation accompanied by the release of latent heat (recalescence).¹³ Extensive studies during the past decades have shed light on the icing physics governing sessile droplet icing,¹⁴⁻¹⁷ condensation frosting,^{18,19} and impact droplet icing.^{20,21} The developed understanding, in turn, contributes to the development of various icephobic surfaces such as superhydrophobic/biphilic surfaces,^{22,23} liquid or solid-state slippery surfaces,²⁴ and gel-type or polymer-based low-toughness surfaces²⁵⁻²⁷ that can regulate ice accretion by removing supercooled droplets before freezing, delaying ice nucleation, and reducing ice adhesion.

Despite the rapid growth of knowledge in icing physics and icephobic surface design, most of the studies on icing confined themselves within atmospheric conditions with little attention being put on the environmental effects beyond temperature. Different from atmospheric icing, droplet icing in a low environment pressure has a higher vaporization flux over the droplet interface, leading to substantial supercooling that enables fast icing from the free surface of the droplet. Previous work has reported that droplet icing can behave so differently under a low-pressure environment,¹³ showing that icing droplets can depart from the surface by vaporizing intensively beneath the droplet due to recalescence that creates an overpressure within the microstructures of superhydrophobic surfaces.¹³ Besides, self-detachment of icing droplets can be achieved via preferential nucleation on the droplet's free surface that produces a concentric inward growth of freezing front, displacing the liquid within the ice shell and leading to a self-dislodging²⁸ and even explosion.²⁹

Regardless of these remarkable observations of self-detachment of icing droplets under low pressures, the ice detaching mechanism remains to be further clarified. Specifically, the prevailing overpressure model²⁸ attributes the droplet jumping to the local vaporization facing the substrate at the end of icing while ignoring the vaporization accompanied by ice propagation. The latter has been shown to introduce intensive outward vapor flow,³⁰ which may also contribute to

droplet detachment. Furthermore, the proposed overpressure model assumes a vaporization flux inversely dependent on the microstructures thus leading to an infinite overpressure when the structure scale reduces to infinitely small,¹³ which is unphysical. More importantly, the icing-droplet detaching kinetics (velocity and direction), key to understanding the icing physics, remain to be investigated.

Here, we demonstrate an unexplored aspect of the mechanisms governing icing-droplet jumping on superhydrophobic surfaces under a rapidly depressurized environment. In addition to causing the previously reported substrate-mediated overpressure, we show that the icing of a supercooled droplet also leads to a strong vaporization momentum due to the progressive propagation of the icing front. The collaborative contribution of the bottom-up (overpressure) and top-down (progressive vaporization) is characterized by the compressive deformation of the icing droplet followed by icing propagation-dependent jumping. By performing droplet icing on superhydrophobic surfaces having differing structures and characterizing droplet jumping dynamics, we develop a model to incorporate the vaporization momentum, which allows us to quantify droplet jumping velocity and direction.

Figure 1a shows the experimental setup to study icing and departure dynamics of supercooled droplets at low pressures (see also Figure S1, Section S1 of Supporting Information for more details on experimental setup and conditions). A deionized water droplet (6-30 μL) was initially deposited on a horizontal superhydrophobic substrate. The superhydrophobic substrate has an apparent advancing contact angle $\theta_a^{\text{app}}=163.2\pm1.8^\circ$ and an apparent receding contact angle $\theta_r^{\text{app}}=158.8\pm1.6^\circ$ (see Figure S3, Section S2 of Supporting Information). After equilibrating at standard room temperatures and pressures (STP) for ≈ 2 min, the droplet and substrate were transferred to a customized chamber for depressurization tests. The vacuum chamber was coupled to a mechanical pump (Agilent DS 602 Rotary Vane Pump) to achieve fast depressurization from atmospheric pressure (101 kPa) to ~ 100 Pa within 10-20 s (Figure 1b). The depressurization rate is 0.1 bar/s, comparable with the previous study (see Figure S1b, Section S1 of Supporting Information).¹³ High-speed optical (PCO.DIMAX CS3) and thermal (FLIR SC7700) imaging was performed from a side view and a top view to capture the droplet icing and jumping dynamics.

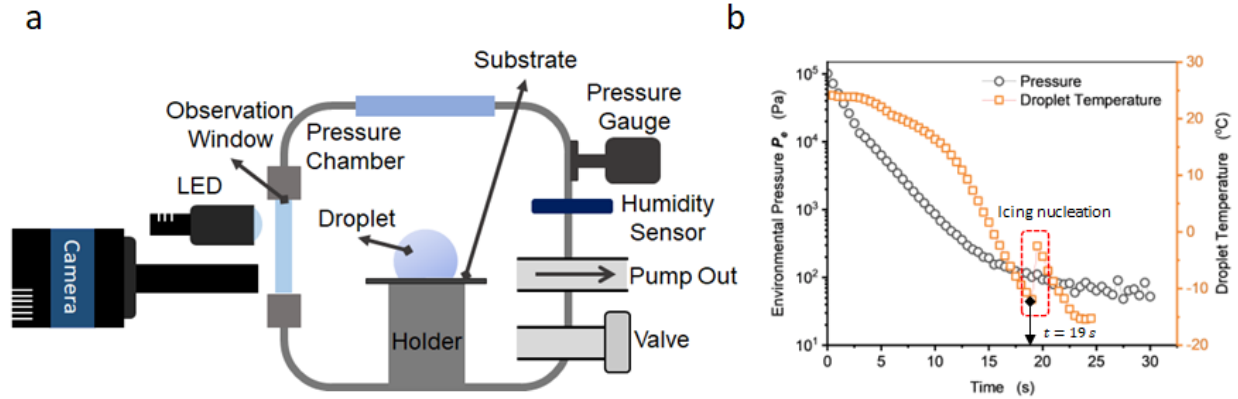


Figure 1. (a) Schematic of the experimental setup for the ice jumping visualization. The water droplet is placed on the substrate which is fixed on the substrate holder. The high-speed camera is used to capture the droplet icing dynamics. The environmental pressure is measured by the pressure gauge. The sapphire window allows for optical and thermal (mid-wave infrared, 1.5-5 μm) imaging. (b) Chamber pressure and droplet temperature as a function of time during chamber depressurization. Droplet temperature is measured by inserting a thermocouple into the droplet residing on the substrate. As the chamber pressure decreases from 101 kPa to ~ 100 Pa, the droplet is supercooled to reach a temperature of around -12°C and then suddenly heats up to $\sim 0^\circ\text{C}$, indicating the occurrence of freezing and recalescence (marked by red dotted frame). See Figures S1 and S2, Section S1, Supporting Information for details on experimental setup and procedures as well as thermodynamic conditions.

Due to the evaporative cooling at the liquid-gas interface (a heat flux up to 50 kW/m^2 , see Figure S1d, Section S1 of Supporting Information), the droplet surface temperature decreased to a supercooled temperature (below -12°C , Figure 1b) until ice nucleation initiated from the free surface of the droplet (Figure 2a, see Video S1). Upon ice nucleation, the icing front (marked by the yellow boundary and line, $t=2.6 \text{ ms}$ in Figure 2a and $t=5 \text{ ms}$ in Figure 2b) propagated fast along the droplet surface. The icing was accompanied by the rapid release of latent heat of solidification, which led to recalescence and heating up of the ice-water slurry from supercooled to $\sim 0^\circ\text{C}$ (equilibrium freezing temperature) as indicated by the infrared (IR) imaging (Figure 2c, see Video S2). As the ice shell was formed to enclose the droplet, the droplet underwent compressive deformation from a sphere cap to an ellipse ($t=6.73 \text{ ms}$, Figure 2a), followed by the self-detachment of the solidifying droplet from the substrate ($t=9.33 \text{ ms}$, Figure 2a). In addition to out-of-plane jumping, the icing droplet also experienced in-plane movement depending on the progressive icing, as confirmed by the top-view visualization (Figure 2b, see Video S1).

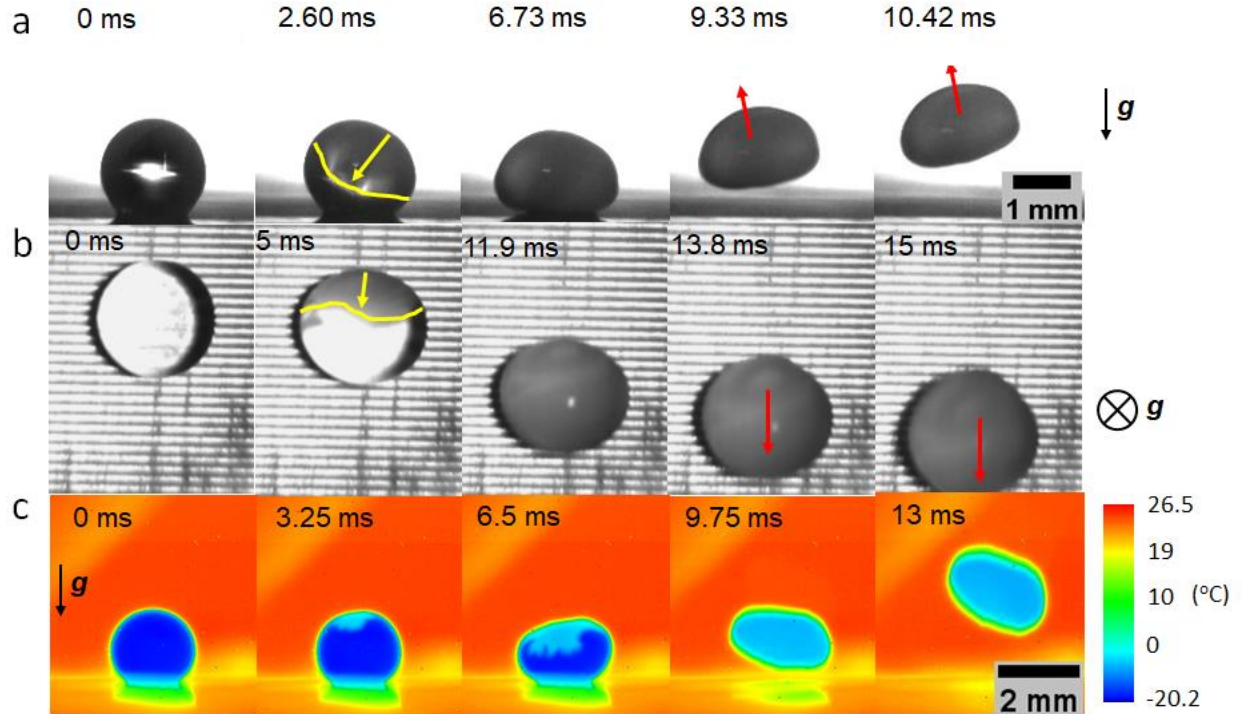


Figure 2. (a) Side-view and (b) top-view high-speed time-lapse images of a 10 μL water droplet solidifying and jumping on micro/nanostructured superhydrophobic surfaces upon depressurization. The yellow lines and arrows indicate the position of the freezing front and the freezing propagation direction, whereas the red arrows indicate the jumping direction of the icing droplet. (c) Side-view thermography of an icing and jumping droplet, showing the ice nucleation and propagation (light blue) over the free surface of the droplet (dark blue). The direction of gravity is indicated by the arrows in (a) and (c) or the circled cross in (b) (gravity pointing to the paper plane). See Videos S1 and S2.

In contrast to the previously reported icing droplet levitation induced by local overpressure underneath the droplet on microstructured superhydrophobic surfaces,²⁸ the observed droplet jumping here is characterized by the droplet compressive deformation and icing propagation-dependent jumping dynamics. We thus propose a physical model to account for the deformation and jumping of the icing droplet, i.e., the vaporization-deformation-bouncing model as illustrated in Figure 3. The primary assumption is the intensive release of vapor from the progressive recalescing surface, which leads to propulsion towards the ice shell, pushing the liquid to deform. The concentric and inward growth of the ice shell leaves the inner of the droplet partially unfrozen as the droplet deforms towards the substrate. Mediated by this unfrozen portion of the droplet interacting with the superhydrophobic substrate, the deformation momentum is accumulated and eventually redirected to propel out-of-plane droplet jumping, in a similar way to droplet impact and bouncing.³¹

To understand the intensive vaporization assumed in our physical model, we first quantified the vaporization flux resulting from recalescence during icing. The vaporization flux (J) is driven by vapor pressure difference, as revealed by the Schrage equation $J \sim \left(\frac{P_d}{\sqrt{T_d}} - \frac{P_e}{\sqrt{T_e}} \right)$,^{32,33} where P_d and T_d are the local vapor pressure and temperature at the droplet interface (ice or water), respectively; P_e and T_e are the environmental pressure and temperature, respectively. Using T_d , P_e , and T_e measured at the moment of ice nucleation, we demonstrated that the normalized vaporization flux reaches a maximum at the recalescing surface around the icing front and is $\sim 10\times$ larger than that at the supercooled water surface (Figure 3b), i.e., $J_i \sim 10J_w$, where J_i is the mass flux at the recalescing surface, and J_w is the mass flux at the supercooled droplet surface. See Section S5, Supporting Information for detailed calculations of vaporization fluxes. The non-uniform vaporization results from the temperature and vapor pressure difference at the icing and supercooled liquid water surfaces,³⁰ and the vaporization flux contrast represents a pulse vapor flow as icing proceeds. Indeed, the strong vapor pulse during recalescence was confirmed by a flow indicator placed next to the icing droplet (Figure S4, Section S3, Supporting Information), consistent with previous observations.³⁰

The observed strong progressive vaporization implies counteractive momentum acting on the icing surface, termed vaporization momentum here, which is believed to be responsible for the compressive deformation and jumping directionality of icing droplets on superhydrophobic surfaces. As a direct confirmation of the vaporization momentum, we performed droplet icing on a slippery surface having a low contact angle hysteresis ($\theta_a^{\text{app}} - \theta_r^{\text{app}} < 8.5^\circ$).³⁴ The use of slippery surfaces allows us to eliminate surface structuring and superhydrophobicity which may be coupled with the droplet icing and jumping dynamics as is the case with overpressure-induced droplet jumping.²⁸ Upon depressurization-induced icing, the droplet slides on the surface in the direction along icing propagation (Figure S5, Section S3, Supporting Information). The observed droplet sliding on slippery surfaces along with the droplet deformation on superhydrophobic surfaces indicate the universality of the vaporization momentum of icing droplets at low pressures. Similar to the vaporization momentum mechanism proposed here, evaporation momentum has been also identified in boiling where fast evaporation of heated liquid deforms growing bubbles.³⁵

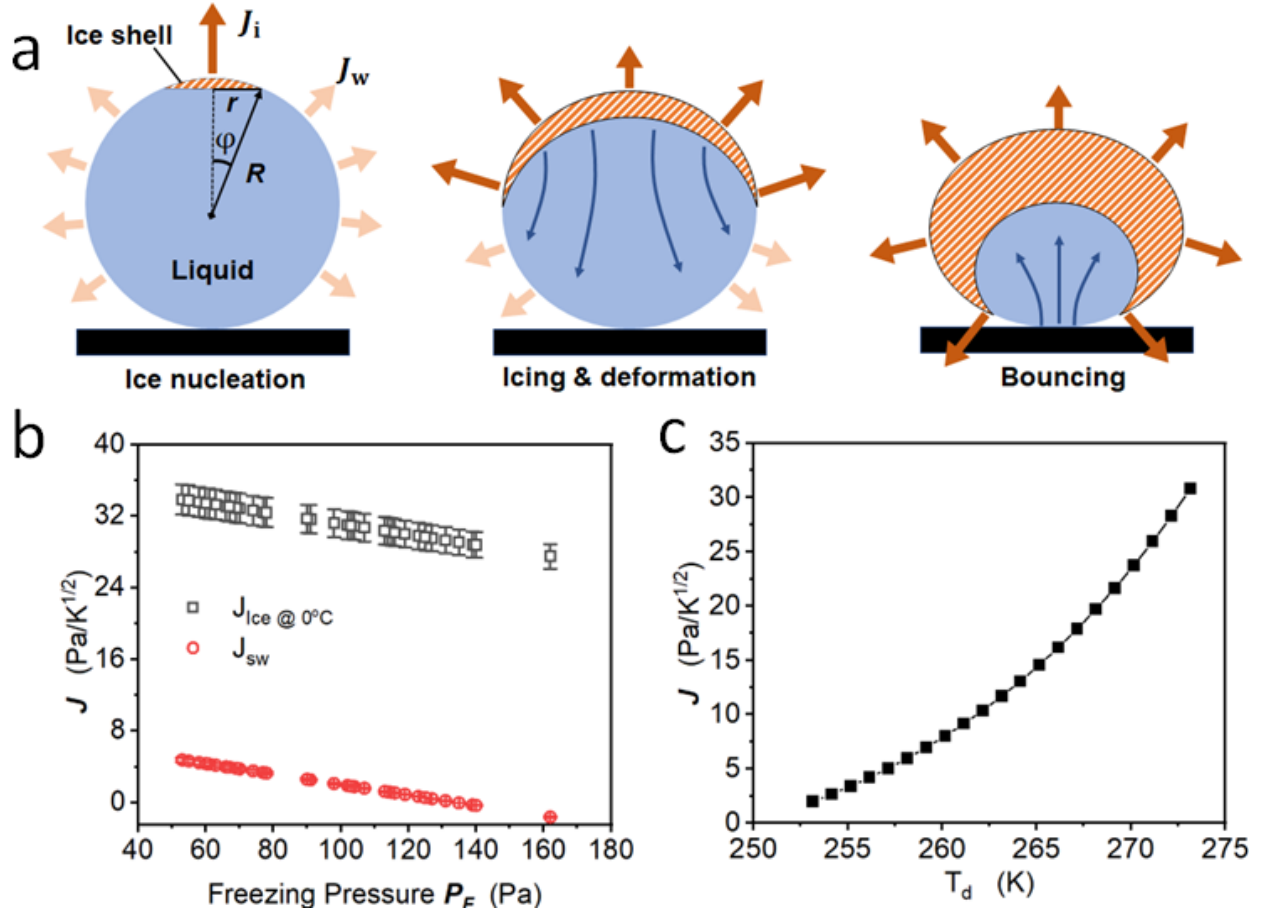


Figure 3. Progressive vaporization of the icing droplet. (a) Schematic showing the cross-section of the icing droplet. Ice shell (orange hatched) forms and propagates over the free surface of the droplet. The recalescence elevates the local temperature around the icing front and leads to a higher vaporization flux (J_i , red arrows) than that of the supercooled droplet surface (J_w , light orange arrows). The flow field within the enclosed water space (light blue) is indicated by dark blue arrows. The length of the arrows indicates the intensity of vaporization (not to scale). As icing proceeds, the droplet is deformed due to the propulsion effects induced by asymmetric vaporization. The substrate counteraction towards the confined liquid redirects the momentum to enable droplet bouncing. (b) The normalized vaporization flux at recalescent ice and supercooled water (sw) surfaces for different environmental pressures. (c) The normalized vaporization flux for different temperature of supercooled droplet

Having identified the role of vaporization momentum in droplet deformation, we then consider if the resulting momentum contributes to droplet jumping. We first analyzed the time scale of droplet detachment Δt_d , defined as the time duration starting from ice nucleation to droplet-substrate separation. Visualization of droplet icing suggests that the ice shell almost encloses the droplet at the droplet detachment moment, though with a small visible portion remains unfrozen upon detachment (Figure 2). Droplet icing experiments on superhydrophobic surfaces having various microstructures (Figure 4a) show Δt_d scales with the inertial-capillary time^{41,42}

$\tau_c = \sqrt{\rho_w R_d^3 / \sigma}$ with a prefactor of ≈ 2.2 (Figure 4b, see Section S7, Supporting Information), where ρ_w is the density of water, R_d is droplet spherical radius, and σ is the surface tension of water. The detaching time ($\Delta t_d \approx 2.2\tau_c$) coincides with the contact time of a low-deformation impact droplet on superhydrophobic surfaces ($\pi/\sqrt{2} \approx 2.2$),⁴³ suggesting the droplet deformation and detaching dynamics demonstrated here are also likely to be dominated by the inertia and capillary forces of the liquid core, regardless of the solidifying ice shell that gradually encloses the liquid domain of the droplet.

Given the unfrozen liquid core inside the icing droplet, we assume the icing droplet deformation and jumping an elastic droplet bouncing process,⁴⁰ where the majority of the vaporization momentum is transferred through the ice shell to the droplet bouncing momentum as the compressive liquid portion elastically interacts with the superhydrophobic substrate. The deformation-bouncing dynamics associated with the liquid core allow us to estimate the possible maximum contribution of vaporization momentum to droplet jumping via the momentum equation:

$$\int_0^{t_d} F_v \cdot dt = \bar{F}_v \Delta t_d = m_d v_j, \quad (1)$$

where F_v is the vaporization propulsion force exerted on the recalescing surface, \bar{F}_v is the average vaporization propulsion force over the detachment time Δt_d , m_d and v_j are the mass and translational velocity of the jumping ice droplet, respectively. Given the limited mass loss due to vaporization during the short freezing time, $m_d \approx \rho_w V_d$, where ρ_w and V_d ($\sim R_d^3$) are the density and volume of the initial water droplet, respectively. Note that gravity is neglected given the droplet' Bond number ($Bo = 0.08 - 0.18 < 1$).

The vaporization propulsion force scales with the released gas velocity and mass flux, i.e., $F_v \sim J_i A_r v_i$, where the vaporization mass flux J_i of the icing surface is constant for a given system and local vapor pressure.^{32,33} v_i is the ejecting velocity of the vapor and A_r ($\sim R_d^2$) is the surface area of the recalescence surface. Here we ignore the momentum contributed by the vaporization of supercooled liquid due to the significantly lower vaporization mass flux compared to the

recalescing surface ($J_i \gg J_w$, Figure 3b). Noting that $\Delta t_d \approx 2.2\tau_c \sim R_d^{1.5}$, Equation 1 is then simplified to $v_j \sim \sqrt{R_d}$ (see Section S7, Supporting Information for detailed derivation). We note that this scaling relationship only represents the upper limit of the jumping velocity as the solidification is assumed not to reduce the bouncing momentum.

To experimentally characterize droplet jumping, we performed droplet (6 to 30 μL) icing experiments on superhydrophobic surfaces with varying microstructures (labeled as S1, S2, and S3 in Figure 4a), characterized by a solid fraction with respect to microstructures ranging from 0.233 to 0.447 and microstructural height ranging from 15 μm to 30 μm . All microstructures are conformally covered by nanostructures having a solid fraction estimated to be 0.108³⁶ (see Section S2, Supporting information) and a characteristic height of 100 nm.³⁷ Surfaces having differing microstructures are specially selected to vary the local overpressure underneath the icing droplet, which is shown by previous studies to govern icing droplet self-jumping.³⁰ The high-speed droplet jumping process was captured to extract the jumping velocity and direction by tracing the droplet trajectory (see Section S4, Supporting Information).^{38,39}

Figure 4c shows the experimentally obtained jumping velocity as a function of the root of the droplet radius, showing a linear trend as revealed by the scaling $v_j \sim \sqrt{R_d}$. The scaling analysis shows that a larger droplet size leads to a higher ice jumping velocity, given that the gravity can be ignored under a low Bond number (<1) where surface tension dominates over gravity forces.

So far, the momentum analysis above only considers the progressive vaporization and does not exclude the role of local overpressure in droplet jumping. To further justify our hypothesis that the vaporization momentum dominates over the local overpressure, we calculated the surface structure-dependent overpressure below the freezing droplet based on the balance of local vaporization and vapor drainage:

$$\Delta P = \frac{J_i R_B^2}{\left(\frac{2h}{3(\Delta P + P_{\text{am}})} \sqrt{\frac{3R_g T}{\pi M}} + \frac{1}{12\mu} F H^3 \right) 4\rho_v}, \quad (2)$$

where R_B is the contact radius of the droplet, H is the height of the surface structure, T is the local temperature and is assumed to be the icing surface temperature T_d , P_{am} is the ambient pressure,

R_g is the universal gas constant, ρ_v is the density of the vapor, μ is the viscosity of the vapor, and M is the molecular mass of water vapor. We note that the mass flux released from the recalescing surface (J_i) is used since the droplet detaching happens only after the icing front approaches the droplet base. Equation 2 is a modified version of the semi-analytical correlation given by Ref. 13 to incorporate the slip flow and Knudsen diffusion effects associated with both micro and nanostructures⁴⁴ (see Section S6, Supporting Information) while the original version fails when the surface structure length scale reduces to nanoscale. Our refined model addresses this limit by coupling the local pressure/temperature and local vaporization flux to the surface structures, and thus can consistently calculate the overpressure contributed by surface structures having different length scales. The jumping velocity is obtained using the momentum equation having a similar form to Equation 1 by taking the calculated local overpressure as the average overpressure underneath the droplet given the short timescale of the development of the overpressure¹³ (see Section S6, Supporting Information for detailed derivation). To validate our overpressure model, we applied Equation 2 to the previously reported experiments¹³ and good agreement was demonstrated (Section S4, Supporting Information).

The droplet detaching velocity calculated by the modified overpressure (Equation 2) is shown to underestimate the droplet jumping velocity in our experiments (see Figure S6, Section S6, Supporting Information). More importantly, the local overpressure-induced jumping velocity is predicted to be highly sensitive to substrate structure length scales, and a smaller jumping velocity is gained for surfaces having smaller solid fractions (Figure S6). However, we observe little dependence on jumping velocity on surface micropatterns (pillars or grooves) and solid fractions (ϕ_{micro} ranging from 0.22 to 0.447) (Figure 4c). The discrepancy between the overpressure theory and experiments suggests the limited role played by the local overpressure in droplet jumping in our experiments.

To further compare the contribution of the progressive vaporization and local overpressure, we quantified the vaporization momentum in contrast to the overpressure momentum and showed that the maximum vaporization momentum (Equation 1) is 2-3X higher than the overpressure momentum (derived from Equation 2) when the ambient pressure at the freezing moment is below 500 Pa (see Figure S6, Section S6, Supporting Information). This justifies the hypothesis when performing the scaling analysis based on the vaporization-deformation-bouncing dynamics

($v_j \sim \sqrt{R_d}$), where the vaporization momentum dominates over the local overpressure. However, we anticipate that the local overpressure to dominate for ambient pressure over 1000 Pa as is the case with previous studies.¹³

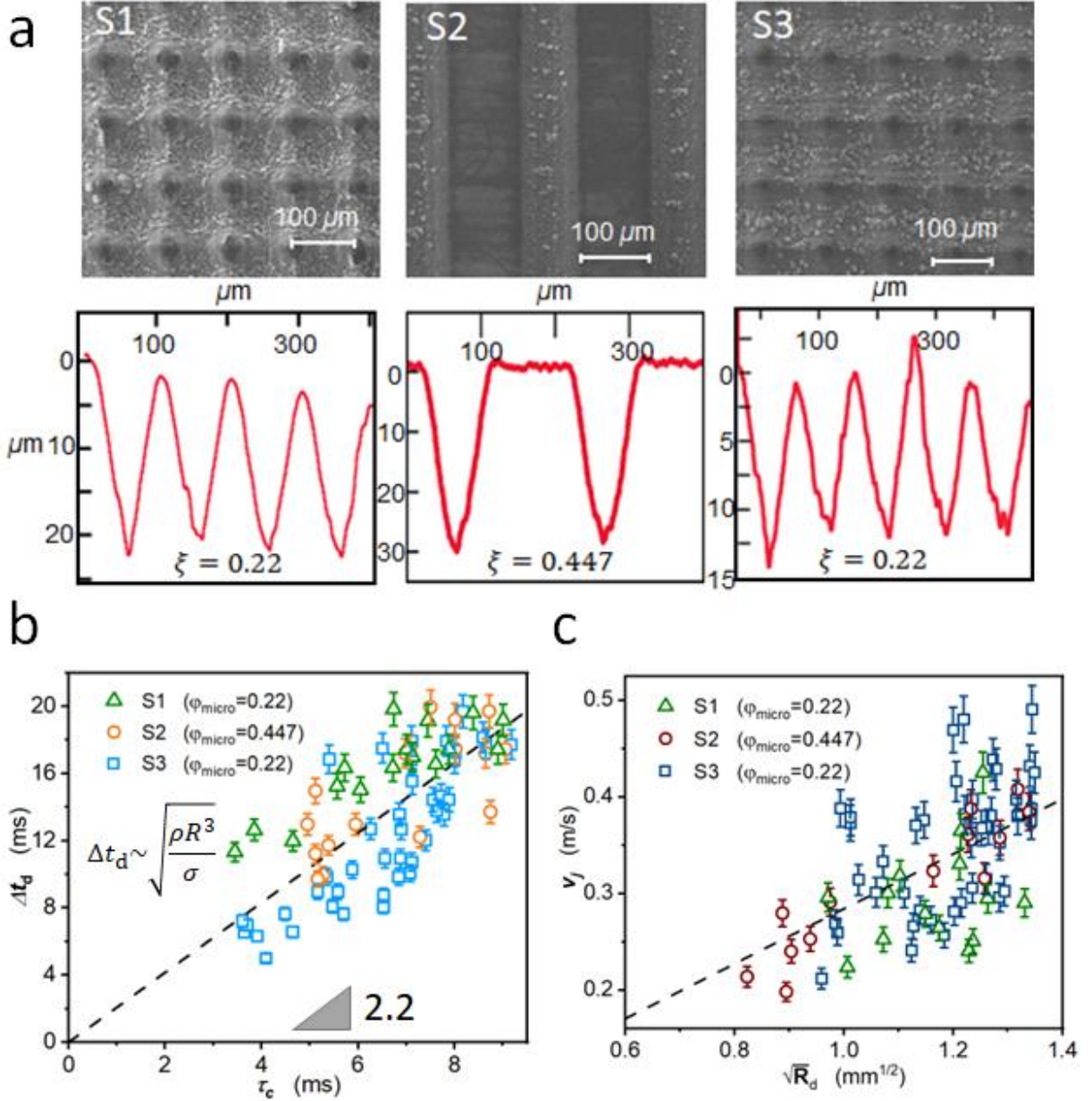


Figure 4. (a) Scanning electron microscopy (SEM) of micro/nanostructured substrates, labeled S1, S2, and S3, along with their cross-section profiles below the SEM images. Solid fractions associated with microstructures (ϕ_{micro}) are presented in the cross-section profiles. (b) Detachment time Δt_d as a function of capillary time τ_c for droplets having various spherical radii (R_d , measured immediately before icing) on different substrates. The dotted line represents the linear fitting with a slope of 2.2. (c) Droplet jumping velocity v_j as a function of the square-rooted droplet spherical radius $\sqrt{R_d}$ for different substrates. See Section S2 for more details on the substrates.

The vaporization momentum is further shown to govern the jumping direction. Since the initial nucleation site represents the start of progressive recalescence, it determines the spatial distribution of vaporization fluxes over the droplet surface and thus the jumping direction. We define the jumping direction by the jumping angle (θ_j) with respect to the substrate normal line at the detaching moment, which is obtained by the jumping trajectory analysis³¹ (see Section S4, Supporting information). The angular position (θ_N) of the initial ice nucleation site with respect to the droplet center of mass (COM) is used to characterize the spatial distribution of ice nucleation (Figure 5a). It was shown that θ_j is linearly correlated with ω_N independent of droplet sizes and substrates, i.e., $\theta_j = -\theta_N$ (Figure 5b). Figure 5c demonstrates a droplet with an ice nucleation initiation position on the right-top interface of the droplet ($\theta_N = -34.2^\circ$), while the icing droplet jumps towards left-top (e.g., $\theta_j = 30.3^\circ$). Consistent with our momentum transfer analysis above, the vaporization momentum is redirected to form the jumping momentum as the liquid phase of the droplet interacts with the substrate in an elastic bouncing-like manner.^{39,45} As a result, the jumping direction is determined by the reflection of the vaporization momentum that pushes the droplet to deform. The jumping directionality observed here, which cannot be explained by the overpressure mechanism,¹³ thus further highlights the significant role of vaporization momentum in icing droplet jumping.

The ice nucleation position and therefore the jumping direction is experimentally observed to be probabilistic. By statistically sampling the data from repeated experiments, we found that the distribution of jumping direction (and ice nucleation position), quantified by the relative frequency ϕ , follows the Gaussian density function (Figure 5d), which reveals that the droplet is more probable to jump perpendicularly to the substrate ($\theta_j \approx 0^\circ$) and less probable to jump in plane ($\theta_j \approx \pm 90^\circ$). This is because ice nucleation tends to initiate at the top of the supercooled droplet, where the temperature is the lowest according to the evaporation heat transfer prediction.^{32,33} Furthermore, the symmetry of the jumping direction distribution suggests that the icing droplet holds an equal probability of jumping leftwards and rightwards, indicative of the minimal effects of experimental conditions (e.g., airflow during vacuuming) on droplet icing and jumping.

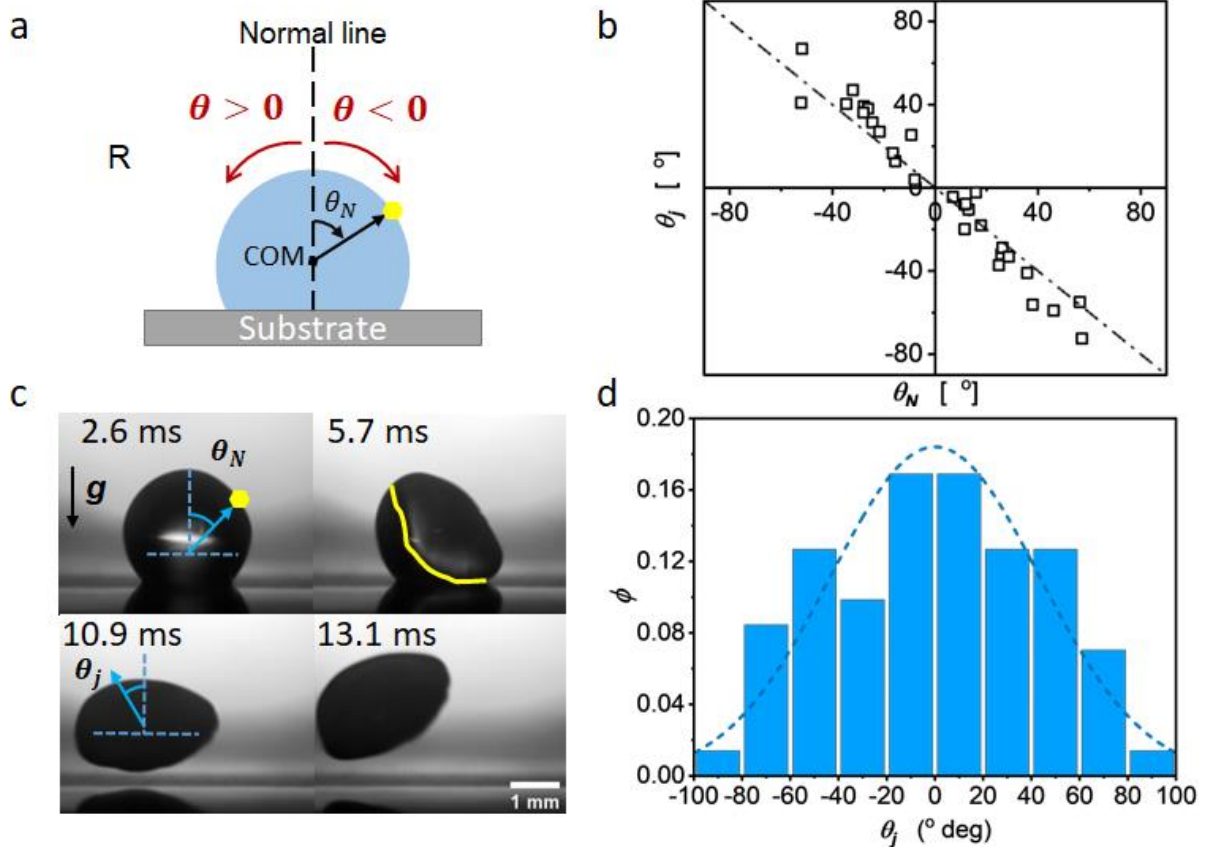


Figure 5. (a) Schematic showing the definition of jumping angle (θ_j) and the angular position of the nucleation site (θ_N). The normal line with respect to the substrate represents $\theta_j=0^\circ$ or $\theta_N=0^\circ$. An angle towards to right is defined to be positive and vice versa. (b) Jumping angle θ_j as a function of the angular position of the ice nucleation site θ_N , showing a linear trend, i.e., $\theta_j=-\theta_N$. (c) An example demonstrating the relationship of jumping angle θ_j and angular position of the nucleation site θ_N . The nucleation site is marked by a hexagon. (d) The relative frequency ϕ of the jumping angle θ_j , which is fitted using a Gaussian density function, $\phi = \frac{1}{43.3\sqrt{2\pi}} e^{-0.5\left(\frac{\theta_j}{43.3}\right)^2}$, with a mean at $\approx 0^\circ$ and a standard deviation of $\approx 43^\circ$, represented by the dotted curve.

In conclusion, we have demonstrated the physics governing supercooled water droplet icing and jumping from superhydrophobic surfaces at low pressures (~ 100 Pa). Although observed at a high depressurization rate (100 kPa to 0.1 kPa within ~ 10 seconds), the icing and droplet self-detaching phenomena indicate a universal mechanism with respect to droplet and surface interaction coupled with vaporization momentum. Different from the previously reported local overpressure underneath the droplet that drives droplet trampolining, the vaporization momentum arises from the globally asymmetric vaporization flux and imparts a counteractive force to the free surface of the icing droplet, leading to the compressive deformation of the droplet as ice front

propagates. We quantified this vaporization momentum in comparison with the local overpressure and showed that the former dominates at ambient pressures of ~ 100 Pa. We proposed a vaporization-compression-bouncing physical model to depict the droplet icing and jumping dynamics, which enables us to predict the jumping velocity as a function of droplet size. Furthermore, the physical model also reveals that the spatially probabilistic nature of the ice nucleation site governs the jumping direction, as confirmed by the experimental statistics. At a higher pressure approaching ~ 1000 Pa, we anticipate the local overpressure mechanism to play a more important role than the vaporization momentum due to the reduced vaporization flux. At such conditions, the coupling between the top-down and bottom-up mechanisms demands further investigation. Our study provides insights into the phase change of supercooled water droplets and presents an approach to detach supercooled droplets from surfaces at decreased pressures. The demonstrated physics may help facilitate water management in vacuum and aerospace-related applications.

ASSOCIATED CONTENT

Supporting Information

The Supporting Information is available free of charge at XXXX.

Fabrication and characterization of the superhydrophobic substrates; Measurement of the droplet freezing temperature; Characterization of ice droplet jumping; Estimation of ice sublimation flux and supercooled water evaporation flux; Quantification of overpressure effect on jumping velocity; Physical model of icing droplet jumping; Calculation of deformation ratio; Estimation of the solid fraction of nanostructure; Ice sliding and rebounding experiment; Characterization of the pressure chamber.

AUTHOR INFORMATION

Corresponding Author

Shuhuai Yao – Department of Mechanical and Aerospace Engineering, The Hong Kong University of Science and Technology, Hong Kong 999077, China; orcid.org/0000-0001-7059-4092; Email: meshyao@ust.hk

Author Contributions

X.Y. and S.A. contributed equally to this work. X.Y., S.A., and S.Y. conceived the idea for the work. X.Y. designed and guided the experiments. S.A., X.Y., S.C., Y.C., N.L, and W.W. performed experiments. G.Z., X.Y., and M.M. fabricated samples for experiments. D.S. performed surface characterization. S.A. and X.Y. analyzed the data, performed modeling, and wrote the manuscript. S.Y. supervised the work and edited the manuscript.

Notes

The authors declare no competing financial interest.

ACKNOWLEDGMENTS

This work was financially supported by the Research Grants Council of Hong Kong under the General Research Fund (16213721). The authors appreciate the help from Dr. Jixiang Wang at Yangzhou University and Prof. Weihong Li at City University of Hong Kong. X.Y. also appreciates Prof. Nenad Miljkovic for his kind support.

References

- (1) Dalili, N.; Edrisy, A.; Carriveau, R. A Review of Surface Engineering Issues Critical to Wind Turbine Performance. *Renewable and Sustainable Energy Reviews* **2009**, *13* (2), 428–438. <https://doi.org/10.1016/j.rser.2007.11.009>.
- (2) Kreder, M. J.; Alvarenga, J.; Kim, P.; Aizenberg, J. Design of Anti-Icing Surfaces: Smooth, Textured or Slippery? *Nat Rev Mater* **2016**, *1* (1), 15003. <https://doi.org/10.1038/natrevmats.2015.3>.
- (3) Alizadeh, A.; Bahadur, V.; Kulkarni, A.; Yamada, M.; Ruud, J. A. Hydrophobic Surfaces for Control and Enhancement of Water Phase Transitions. *MRS Bull* **2013**, *38* (5), 407–411. <https://doi.org/10.1557/mrs.2013.104>.
- (4) Schutzius, T. M.; Jung, S.; Maitra, T.; Eberle, P.; Antonini, C.; Stamatopoulos, C.; Poulikakos, D. Physics of Icing and Rational Design of Surfaces with Extraordinary Icephobicity. *Langmuir* **2015**, *31* (17), 4807–4821. <https://doi.org/10.1021/la502586a>.
- (5) Petty, K. R.; Floyd, C. D. A Statistical Review of Aviation Airframe Icing Accidents in the US. In *Proceedings of the 11th Conference on Aviation, Range, and Aerospace Hyannis*; 2004.
- (6) Philip Appiah-Kubi. U.S Inflight Icing Accidents and Incidents, 2006 to 2010., The University of Tennessee, Knoxville, 2011.
- (7) Yirtici; Ozcan; Ismail H. Tuncer; Serkan Ozgen. Ice Accretion Prediction on Wind Turbines and Consequent Power Losses. *J Phys Conf Ser* **2016**, *753* (2).
- (8) He, Z.; Wang, J. Anti-Icing Strategies Are on the Way. *The Innovation* **2022**, *3* (5), 100278. <https://doi.org/10.1016/j.xinn.2022.100278>.
- (9) Hao, T.; Zhu, Z.; Yang, H.; He, Z.; Wang, J. All-Day Anti-Icing/Deicing Film Based on Combined Photo-Electro-Thermal Conversion. *ACS Appl Mater Interfaces* **2021**, *13* (37), 44948–44955. <https://doi.org/10.1021/acsami.1c13252>.
- (10) Gao, L.; Hu, H. Wind Turbine Icing Characteristics and Icing-Induced Power Losses to Utility-Scale Wind Turbines. *Proceedings of the National Academy of Sciences* **2021**, *118* (42). <https://doi.org/10.1073/pnas.2111461118>.
- (11) Hwang, H.; Ma, K. Y.; Kim, J. W.; Yuk, D.; Hong, J.; Jung, J. H.; Yong, S.-M.; Choi, J.; Kim, J. Y.; Shin, H. S. Radio-Frequency-Transmitting Hexagonal Boron Nitride-Based Anti- and de-Icing Heating System. *Nanoscale* **2020**, *12* (42), 21895–21900. <https://doi.org/10.1039/D0NR06333A>.
- (12) Bai, G.; Gao, D.; Liu, Z.; Zhou, X.; Wang, J. Probing the Critical Nucleus Size for Ice Formation with Graphene Oxide Nanosheets. *Nature* **2019**, *576* (7787), 437–441. <https://doi.org/10.1038/s41586-019-1827-6>.
- (13) Schutzius, T. M.; Jung, S.; Maitra, T.; Graeber, G.; Köhme, M.; Poulikakos, D. Spontaneous Droplet Trampolining on Rigid Superhydrophobic Surfaces. *Nature* **2015**, *527* (7576), 82–85. <https://doi.org/10.1038/nature15738>.
- (14) Jung, S.; Tiwari, M. K.; Doan, N. V.; Poulikakos, D. Mechanism of Supercooled Droplet Freezing on Surfaces. *Nat Commun* **2012**, *3* (1), 615. <https://doi.org/10.1038/ncomms1630>.

- (15) Jung, S.; Tiwari, M. K.; Poulikakos, D. Frost Halos from Supercooled Water Droplets. *Proceedings of the National Academy of Sciences* **2012**, *109* (40), 16073–16078. <https://doi.org/10.1073/pnas.1206121109>.
- (16) Nguyen, V.-H.; Nguyen, B. D.; Pham, H. T.; Lam, S. S.; Vo, D.-V. N.; Shokouhimehr, M.; Vu, T. H. H.; Nguyen, T.-B.; Kim, S. Y.; Le, Q. van. Anti-Icing Performance on Aluminum Surfaces and Proposed Model for Freezing Time Calculation. *Sci Rep* **2021**, *11* (1), 3641. <https://doi.org/10.1038/s41598-020-80886-x>.
- (17) Wang, L.; Tian, Z.; Jiang, G.; Luo, X.; Chen, C.; Hu, X.; Zhang, H.; Zhong, M. Spontaneous Dewetting Transitions of Droplets during Icing & Melting Cycle. *Nat Commun* **2022**, *13* (1), 378. <https://doi.org/10.1038/s41467-022-28036-x>.
- (18) Yang, S.; Wu, C.; Zhao, G.; Sun, J.; Yao, X.; Ma, X.; Wang, Z. Condensation Frosting and Passive Anti-Frosting. *Cell Rep Phys Sci* **2021**, *2* (7), 100474. <https://doi.org/10.1016/j.xcrp.2021.100474>.
- (19) Nath, S.; Boreyko, J. B. On Localized Vapor Pressure Gradients Governing Condensation and Frost Phenomena. *Langmuir* **2016**, *32* (33), 8350–8365. <https://doi.org/10.1021/acs.langmuir.6b01488>.
- (20) de Ruiter, J.; Soto, D.; Varanasi, K. K. Self-Peeling of Impacting Droplets. *Nat Phys* **2018**, *14* (1), 35–39. <https://doi.org/10.1038/nphys4252>.
- (21) Jin, P.; Yan, X.; Hoque, M. J.; Rabbi, K. F.; Sett, S.; Ma, J.; Li, J.; Fang, X.; Carpenter, J.; Cai, S.; Tao, W.; Miljkovic, N. Ultra-Low Ice-Substrate Adhesion and Self-Deicing during Droplet Impact Freezing. *Cell Rep Phys Sci* **2022**, *3* (5), 100894. <https://doi.org/10.1016/j.xcrp.2022.100894>.
- (22) Puretskiy, N.; Chanda, J.; Stoychev, G.; Synytska, A.; Ionov, L. Anti-Icing Superhydrophobic Surfaces Based on Core-Shell Fossil Particles. *Adv Mater Interfaces* **2015**, *2* (11), 1500124. <https://doi.org/10.1002/admi.201500124>.
- (23) Boinovich, L. B.; Emelyanenko, A. M. Anti-Icing Potential of Superhydrophobic Coatings. *Mendeleev Communications* **2013**, *23* (1), 3–10. <https://doi.org/10.1016/j.mencom.2013.01.002>.
- (24) Wong, T.-S.; Kang, S. H.; Tang, S. K. Y.; Smythe, E. J.; Hatton, B. D.; Grinthal, A.; Aizenberg, J. Bioinspired Self-Repairing Slippery Surfaces with Pressure-Stable Omniphobicity. *Nature* **2011**, *477* (7365), 443–447. <https://doi.org/10.1038/nature10447>.
- (25) Zhuo, Y.; Xiao, S.; Håkonsen, V.; He, J.; Zhang, Z. Anti-Icing Ionogel Surfaces: Inhibiting Ice Nucleation, Growth, and Adhesion. *ACS Mater Lett* **2020**, *2* (6), 616–623. <https://doi.org/10.1021/acsmaterialslett.0c00094>.
- (26) Urata, C.; Nagashima, H.; Hatton, B. D.; Hozumi, A. Transparent Organogel Films Showing Extremely Efficient and Durable Anti-Icing Performance. *ACS Appl Mater Interfaces* **2021**, *13* (24), 28925–28937. <https://doi.org/10.1021/acsaami.1c06815>.
- (27) He, Z.; Wu, C.; Hua, M.; Wu, S.; Wu, D.; Zhu, X.; Wang, J.; He, X. Bioinspired Multifunctional Anti-Icing Hydrogel. *Matter* **2020**, *2* (3), 723–734. <https://doi.org/10.1016/j.matt.2019.12.017>.

- (28) Graeber, G.; Schutzius, T. M.; Eghlidi, H.; Poulikakos, D. Spontaneous Self-Dislodging of Freezing Water Droplets and the Role of Wettability. *Proc Natl Acad Sci U S A* **2017**, *114* (42), 11040–11045. <https://doi.org/10.1073/pnas.1705952114>.
- (29) Wildeman, S.; Sterl, S.; Sun, C.; Lohse, D. Fast Dynamics of Water Droplets Freezing from the Outside In. *Phys Rev Lett* **2017**, *118* (8), 084101. <https://doi.org/10.1103/PhysRevLett.118.084101>.
- (30) Graeber, G.; Dolder, V.; Schutzius, T. M.; Poulikakos, D. Cascade Freezing of Supercooled Water Droplet Collectives. *ACS Nano* **2018**, *12* (11), 11274–11281. <https://doi.org/10.1021/acsnano.8b05921>.
- (31) Yan, X.; Qin, Y.; Chen, F.; Zhao, G.; Sett, S.; Jahidul Hoque, M.; Fazle Rabbi, K.; Zhang, X.; Wang, Z.; Li, L.; Chen, F.; Feng, J.; Miljkovic, N. Laplace Pressure Driven Single-Droplet Jumping on Structured Surfaces. *ACS Nano* **2020**, *14* (10), 12796–12809. <https://doi.org/10.1021/acsnano.0c03487>.
- (32) Pan, Z.; Dash, S.; Weibel, J. A.; Garimella, S. v. Assessment of Water Droplet Evaporation Mechanisms on Hydrophobic and Superhydrophobic Substrates. *Langmuir* **2013**, *29* (51), 15831–15841. <https://doi.org/10.1021/la4045286>.
- (33) Nguyen, T. A. H.; Biggs, S. R.; Nguyen, A. v. Analytical Model for Diffusive Evaporation of Sessile Droplets Coupled with Interfacial Cooling Effect. *Langmuir* **2018**, *34* (23), 6955–6962. <https://doi.org/10.1021/acs.langmuir.7b03862>.
- (34) Zhao, H.; Deshpande, C. A.; Li, L.; Yan, X.; Hoque, M. J.; Kuntumalla, G.; Rajagopal, M. C.; Chang, H. C.; Meng, Y.; Sundar, S.; Ferreira, P.; Shao, C.; Salapaka, S.; Sinha, S.; Miljkovic, N. Extreme Antiscaling Performance of Slippery Omniphobic Covalently Attached Liquids. *ACS Appl Mater Interfaces* **2020**, *12* (10), 12054–12067. <https://doi.org/10.1021/acsaami.9b22145>.
- (35) Kandlikar, S. G. Evaporation Momentum Force and Its Relevance to Boiling Heat Transfer. *J Heat Transfer* **2020**, *142* (10). <https://doi.org/10.1115/1.4047268>.
- (36) Stamatopoulos, C.; Milionis, A.; Ackert, N.; Donati, M.; Leudet de la Vallée, P.; Rudolf von Rohr, P.; Poulikakos, D. Droplet Self-Propulsion on Superhydrophobic Microtracks. *ACS Nano* **2020**, *14* (10), 12895–12904. <https://doi.org/10.1021/acsnano.0c03849>.
- (37) Zhao, G.; Zou, G.; Wang, W.; Geng, R.; Yan, X.; He, Z.; Liu, L.; Zhou, X.; Lv, J.; Wang, J. Competing Effects between Condensation and Self-Removal of Water Droplets Determine Antifrosting Performance of Superhydrophobic Surfaces. *ACS Appl Mater Interfaces* **2020**, *12* (6), 7805–7814. <https://doi.org/10.1021/acsaami.9b21704>.
- (38) Yan, X.; Zhang, L.; Sett, S.; Feng, L.; Zhao, C.; Huang, Z.; Vahabi, H.; Kota, A. K.; Chen, F.; Miljkovic, N. Droplet Jumping: Effects of Droplet Size, Surface Structure, Pinning, and Liquid Properties. *ACS Nano* **2019**, *13*, acsnano.8b06677. <https://doi.org/10.1021/acsnano.8b06677>.
- (39) Yan, X.; Ji, B.; Feng, L.; Wang, X.; Yang, D.; Rabbi, K. F.; Peng, Q.; Hoque, M. J.; Jin, P.; Bello, E.; Sett, S.; Alleyne, M.; Cropek, D. M.; Miljkovic, N. Particulate–Droplet Coalescence and Self-Transport on Superhydrophobic Surfaces. *ACS Nano* **2022**, *16* (8), 12910–12921. <https://doi.org/10.1021/acsnano.2c05267>.

- (40) Richard, D.; Clanet, C.; Quéré, D. Contact Time of a Bouncing Drop. *Nature* **2002**, *417* (6891), 811–811. <https://doi.org/10.1038/417811a>.
- (41) Yu, X.; Zhang, Y.; Hu, R.; Luo, X. Water Droplet Bouncing Dynamics. *Nano Energy* **2021**, *81*, 105647. <https://doi.org/10.1016/j.nanoen.2020.105647>.
- (42) Liu, F.; Ghigliotti, G.; Feng, J. J.; Chen, C.-H. Numerical Simulations of Self-Propelled Jumping upon Drop Coalescence on Non-Wetting Surfaces. *J Fluid Mech* **2014**, *752*, 39–65. <https://doi.org/10.1017/jfm.2014.320>.
- (43) Rayleigh, Lord. VI. On the Capillary Phenomena of Jets. *Proceedings of the Royal Society of London* **1879**, *29* (196–199), 71–97. <https://doi.org/10.1098/rspl.1879.0015>.
- (44) Darabi, H.; Ettehad, A.; Javadpour, F.; Sepehrnoori, K. Gas Flow in Ultra-Tight Shale Strata. *J Fluid Mech* **2012**, *710*, 641–658. <https://doi.org/10.1017/jfm.2012.424>.
- (45) Aboud, D. G. K.; Kietzig, A.-M. On the Oblique Impact Dynamics of Drops on Superhydrophobic Surfaces. Part II: Restitution Coefficient and Contact Time. *Langmuir* **2018**, *34* (34), 9889–9896. <https://doi.org/10.1021/acs.langmuir.8b01233>.

Table of Content

